Physics of Plasmas

Enhancing cylindrical compression by reducing plasma ablation in pulsed-power drivers

Cite as: Phys. Plasmas **26**, 042706 (2019); https://doi.org/10.1063/1.5086305
Submitted: 19 December 2018 . Accepted: 04 March 2019 . Published Online: 17 April 2019

P.-A. Gourdain, M. B. Adams, M. Evans, H. R. Hasson, R. V. Shapovalov, J. R. Young, and I. West-Abdallah

Physics of Plasmas ARTICLE scitation.org/journal/php

Enhancing cylindrical compression by reducing plasma ablation in pulsed-power drivers

Cite as: Phys. Plasmas **26**, 042706 (2019); doi: 10.1063/1.5086305
Submitted: 19 December 2018 · Accepted: 4 March 2019 ·
Published Online: 17 April 2019

P.-A. Gourdain, M. B. Adams, M. Evans, H. R. Hasson, R. V. Shapovalov, J. R. Young, and I. West-Abdallah

AFFILIATIONS

Department of Physics and Astronomy, University of Rochester, Rochester, New York 14627, USA

ABSTRACT

Warm dense matter, which can be found in planetary cores, is too dense to be described by plasma theory and too hot to be considered condensed matter. With no theory describing perfectly how such large quantum systems evolve at macroscopic scales, modeling planetary evolution is simply out of reach. While recent experiments using high power lasers and heavy ion beams have produced warm dense matter samples, they do not confine matter long enough to allow for bulk material properties to take hold, precluding the validation of any theories beyond electron-ion equilibration time. To this end, pulsed-power drivers are required. This approach allows experimentalists to probe macroscopic states of matter where bulk material properties are at equilibrium. High resolution numerical simulations show that a mega-ampere pulsed-power driver can generate macroscopic samples of warm dense matter, using direct magnetic compression, without any pusher. A thin coating, deposited onto the material just before the experiment, softens the density gradients responsible for plasma ablation. Starved of plasma outside the conductors, electrical currents are forced to flow along material surfaces, resulting in a very stable magnetic topology that yields homogeneous compression above 1 Mbar. Another key aspect is as follows: mega-ampere pulsed power systems are compact enough to be located next to existing high brilliance x-ray sources, which can probe best the properties of matter under extreme pressure.

I. INTRODUCTION

Dense materials brought to electron volt temperatures are typically in the warm dense regime. This state of matter is common to thousands of planets, including gas giants[1,2] and large, rocky exo-planets.[3] Yet, we have limited access to warm dense matter. It is difficult to confine, and its properties are challenging to measure; only x-rays with energies above 20 keV can be used to probe matter this dense. Without a precise understanding of its basic properties, like viscosity or conductivity, planetary evolution cannot be modeled. Posed as a grand challenge to the prediction of planetary habitability, large facilities[4,5] have undertaken a series of successful experiments to measure the properties of warm dense matter and measure its properties.[6–10]

Only then can bulk material properties[11] be compared with theoretical models.[12–14] A key ingredient to reach bulk equilibrium is confinement. At such pressures, macroscopic samples of WDM need to be produced using pulsed-power drivers. Several methods have been proposed to reach such states. Flyer plates[15] on the Z-machine have compressed matter up to 4 Mbar using shock waves. However, shock compression may not lead to equilibrium conditions. Cylindrical pushers were used more recently to reach 10 Mbar using isentropic compression.[16] Cylindrical geometry also offers excellent diagnostic access, and Abel inversion techniques can infer the local properties of matter (e.g., density, temperature,…) from line average measurements. A mega-ampere class pulsed-power driver generating megabar pressures would be extremely attractive since the machine would be small enough to be relocated next to a high-intensity x-ray source. However, using pushers seems prohibitive as they increase the effective mass of the load and reduce the peak pressure a driver can reach for a given current. It was shown that slightly increasing the rise time allowed for larger peak currents, yielding pressures closer to 1 Mbar.[17–19]

In theory, magnetic anvil cells[20] on fast pulsed-power drivers can produce large samples (100 μm) of warm dense matter on relatively long time scales (200 ns) and at relatively low currents (1 MA) without the need of a pusher. In high compression ratio experiments ($R_{initial}/R_{final}>10$), hydrodynamic and magnetohydrodynamic instabilities tend to perturb symmetry.[21] However, the ratios required to produce warm dense matter are much smaller ($R_{initial}/R_{final}<10$), and instabilities become less severe, especially when coating is present.[22,23] In fact, common cylindrical instabilities, like kink modes, are all but absent of magnetic anvil cells.[24]

Perfectly symmetric compression can yield large variations in the final properties of highly compressed matter. Inhomogeneities can simply arise when constraints on the magnetic topology are not enforced, a major impediment in using the field alone to compress

matter. Plasma ablated by large current densities flowing near material surfaces allows currents to flow away from a predetermined path, and the magnetic topology driving the compression diverges from the topology set by the shape of electrodes. Further, the mechanisms responsible for plasma ablation can neither be controlled nor be reproduced, leading to shot-to-shot variations.

If ablation is not controlled early in the discharge, the compression is heterogeneous, leading to samples that cannot be diagnosed correctly using line-average diagnostics. Several methods have been investigated to regain homogeneous compression with magnetic anvil cells. A pre-ionized gas puff was initially used to keep currents away from material surfaces, *de facto* limiting the initial ablation.[24] A low-density foam surrounding the rod was theorized to limit spurious current paths, yielding symmetric compression.[25] However, recent experiments have shown that a thin, spray-on dielectric coating[26] was the most effective method at reducing ablation. Aerosol coating is an attractive approach because of its simplicity.

This paper uses two-fluid simulations to demonstrate that ablation in magnetic anvil cells switches from purely adiabatic expansion to magnetic compression. In the latter regime, current paths are confined near the material surface and lead to homogeneous compression. For the first time, our analysis shows that the initial coating of material surfaces is all it takes to generate macroscopic samples of warm dense matter where variations in material properties are virtually eliminated.

II. ESTIMATION OF THE OUTFLOW SCALE LENGTH IN MAGNETIC ANVIL CELLS

When Ohmic heating is the sole source of energy input, the energy conservation can be written as

$$\frac{Dp}{Dt} - \gamma \frac{p}{\rho}\frac{D\rho}{Dt} = (\gamma - 1)\eta J^2. \tag{1}$$

γ is the ratio of specific heats, p is the plasma pressure, J is the current density, and ρ is the bulk mass density. D/Dt is the convective derivative. Radiation effects can also be ignored in our energy balance as no part of the surface is directly irradiated by intense radiations. Besides Ohmic heating and radiation, other processes (e.g., heat conduction) are also neglected. As justified later by numerical simulations, using constant resistivity across the outflow layer is an acceptable simplification. In this case, the current density can be approximated by

$$J = \frac{I}{2\pi a \delta}, \tag{2}$$

where a is the radius of the sample and δ is the skin depth given by

$$\delta = \sqrt{\frac{2\eta}{\omega \mu_0}}. \tag{3}$$

In this context, ω should be interpreted as the rate of electrical energy injection inside the system, rather than the usual steady state approximation of a system driven at an angular frequency ω. Nonlinear diffusion[27] has also been omitted for the sake of simplicity, and its effect in Z-pinches is usually not negligible.[28] It was shown that the skin depth given by Eq. (3) is a relatively good approximation for a single current pulse,[29] as the one produced by a linear transformer driver (LTD).[30] In dominantly axisymmetric systems, the total current I is simply given by

$$I = \frac{B2\pi a}{\mu_0}. \tag{4}$$

As a result, the ablated mass density rate following the flow is given by

$$\frac{D\rho}{Dt} = \rho\left(\frac{1}{\gamma p}\frac{Dp}{Dt} - \frac{\gamma - 1}{\gamma}\frac{\omega}{\beta}\right). \tag{5}$$

Here, β(r) is the kinetic pressure normalized to the magnetic pressure at the material surface, where r = a. Equation (5) is a specialized version of Eq. (1) applied to z-pinches, under the assumptions listed above. If we suppose the flow steady state, we can simplify the material derivative operator. Using the momentum conservation equation for a one-dimensional flow

$$\frac{\rho v_r}{p}\frac{dv_r}{dr} = -\frac{1}{p}\frac{dp}{dr} + \frac{2}{\beta\delta} \tag{6}$$

and the characteristic pressure scale length $L_P = \left|p\frac{dr}{dp}\right|$, we can define two separate regimes. In regimes where the flow mostly expands adiabatically, the second term on the right-hand side of Eq. (6) is negligible, i.e., $L_P \ll \beta\delta/2$. As a result, the ablated mass density rate along the flow leaving the material surface and feeding the plasma surrounding the sample is given by

$$\frac{D\rho}{Dt} = \rho\frac{1}{\gamma p}\frac{Dp}{Dt}. \tag{7}$$

For steady state flows, this equation gives the characteristic mass density scale length $L_\rho = \left|\rho\frac{dr}{d\rho}\right|$ as

$$L_\rho \sim \gamma L_P. \tag{8}$$

The characteristic mass density scale length is on the order of the pressure characteristic scale length. However, in regimes where β or the skin depth is small, i.e., $L_P \gg \beta\delta/2$, the ablated mass density rate becomes

$$\frac{D\rho}{Dt} = -\rho\frac{\gamma - 1}{\gamma}\frac{\omega}{\beta}. \tag{9}$$

Steady state mass conservation in one dimension

$$v_r\frac{d\rho}{dr} + \rho\frac{dv_r}{dr} = 0 \tag{10}$$

and Eq. (6) produce L_ρ in this regime

$$L_\rho = M_A^2\delta, \tag{11}$$

where M_A is the Alfvénic Mach number. In this regime, the characteristic scale length depends on the mass density via the Alfvén wave speed. While the largest limitation in our approach is the constant resistivity, we have shown that the ablation flow can be in two distinct regimes. In the first regime, when $L_P \ll \beta\delta/2$, the ablation flow scale length follows the pressure scale length. The mass ablation outflow in this regime is purely controlled by thermodynamics processes, and the heating rate is the only control knob. In the second regime, $L_P \gg \beta\delta/2$, mass ablation is ruled by the skin depth (resistivity), the kinetic energy of the flow, and the magnetic energy. All three parameters depend upon three quantities that can be controlled *ab initio*, namely, the ablated material, the magnetic field strength, via the rod radius, and

the resistivity of the material. It also shows that it is critical to switch to the second regime as soon as possible in the discharge to limit the expansion of the ablated flow. According to Eq. (5), mass density and resistivity are the most important control knobs.

We now generalize the discussion to a more realistic situation, using the code PERSEUS,[31] and show how mass density and resistivity impact the ablation outflow in magnetic anvil cells. The resistivity will be taken as constant or follow a simplified version of Lee-More-Desjarlais.[32,33] Unlike regular MHD codes, which use an artificial resistivity in the vacuum region, the Hall effect and electron inertia limit electrical currents in PERSEUS simulations. It is primordial to use electron physics to capture more accurately the ablation outflow since its expansion is sensitive to the physics taking place at the plasma-vacuum interface. We used 50 grid cells across the material sample in this simulation, corresponding to a resolution of 10 μm. PERSEUS is a two-fluid code with one single ion species, and it cannot differentiate between the rod and the coating. We supposed that the compression is done on HADES,[34] a compact pulsed-power device using LTDs to generate 1 MA in 150 ns in small inductance loads. The current rise follows

$$I = I_{peak} sin\left(\frac{\pi}{2}\frac{t}{t_r}\right)\exp\left(-\frac{t}{t_d}\right), \tag{12}$$

where $I_{peak} = 1$ MA, t_r=150 ns, and $t_d = 6\ t_r$.

The initial uncoated aluminum rod has a 600-μm diameter. The coated rod has a diameter of 500-μm and a 100-μm thick coating. The mass density of the coating is four times less than the aluminum mass density. First, we look at the case where resistivity is constant across the whole domain, taken as 10^{-7} Ωm. In this case, the Hall effect and electron inertia keep the current from flowing inside the vacuum.[35] Roughly halfway through the current rise, Fig. 1(a) shows that the ablation layer expanded by 0.2 mm with no coating, compared to 0.075 mm when a coating is present. The mass density change at the edge of the rod is the only difference in both simulations. There is little change when including the Lee-More-Desjarlais resistivity, as shown in Fig. 1(b).

Figure 2 shows the ablation scale length from Eq. (11) at two different times. At the earliest time (t = 48 ns from Fig. 1), there is already a noticeable difference in both ablation scale lengths, with the coated rod having the smallest one. At later times (t = 56 ns and 64 ns), the difference widens. The ablation scale length of the bare sample is on the order of 6 μm, across a layer that is 200 μm wide, near the surface of the sample. The ablation scale length of the coated sample is 2 μm, across a region spanning 80 μm around the aluminum rod. By delaying the ablation, the coating allows the field to be strong enough to overcome the ram pressure of the ablated plasma. The ablation layer simply stops expanding and gets compressed against the rod. A thinner ablation layer keeps electric currents at smaller radii, further strengthening the field, compared to the cases where no coating is present. Simulations clearly show that the ablation scale length L_ρ is larger when conductors are not coated.

III. MAGNETIC ANVIL CELLS USING THIN COATINGS

The generation of warm dense matter using pulsed-power drivers, while promising, has seen some setbacks. The biggest problem comes from the ablation plasma, which generates spurious current paths around the sample. These uncontrolled current channels are not

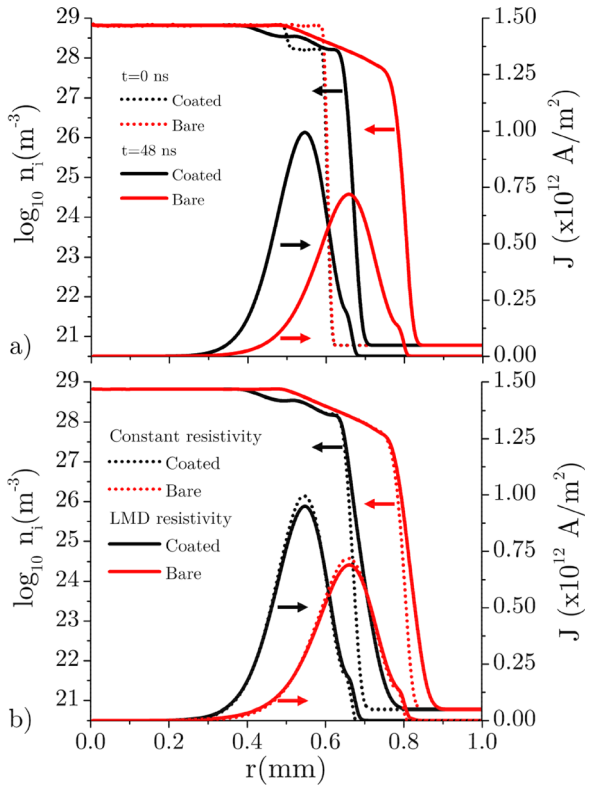

FIG. 1. (a) The initial density profile, shown on the $\log_{10}$ scale (left axis), can be easily compared with the same profile, 48 ns later. The ablated material region (r > 0.6 mm) has well expanded into the vacuum. However, when a coating is present, the expansion region is thrice as narrow compared to the case where no coating was used. The resulting current density, plotted on the linear scale (right axis), is higher and is 30% closer to the axis of symmetry, yielding a magnetic pressure almost twice as high. This case used a constant resistivity of 10^{-7} Ω/m throughout the domain. (b) We observe enhanced expansion in the outmost layers of the ablated material when using Lee-More-Desjarlais resistivity.

only nefarious to the quality of the compression but can also generate plasmas hot enough to clamp the ablation in the first regime, using magnetic pressure to compress a hot plasma, instead of the material sample. As a result, understanding how the coating impacts the ablation layer can greatly improve the quality of the compression obtained by magnetic anvil cells. Using PERSEUS, we now model a complete magnetic anvil cell in two dimensions, including the top and bottom electrodes, using the current waveform delivered by HADES. While the current rise follows the same time evolution, we have now decreased the overall resolution to 70 μm to accommodate the larger simulation volume. The model is shown in Fig. 3, albeit in three dimensions for clarity.

In this section, all rods have a diameter of 1 mm and a length of 5 mm. As before, we first use an aluminum rod devoid of coating. Figure 4(a) shows a small portion of the computational domain, centered on the bare rod. The left side of Fig. 4(a) shows the current density, and the right side shows the ion number density, both on the logarithmic scale. In regions where the ablation has been quenched numerically, by setting surface flows to 0, the current remains close to

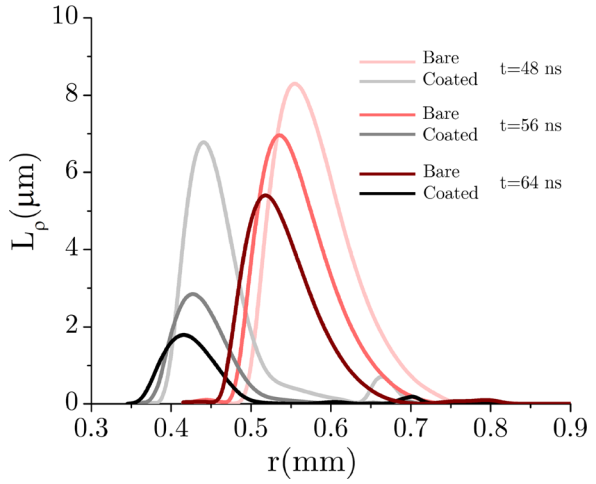

FIG. 2. The ablation scale length $L\rho$ as computed by PERSEUS, using Lee-More-Desjarlais resistivity, at 48 ns, 56 ns, and 64 ns into the current rise, well before implosion. The scale length is clearly smaller when a coating is used and decreases more rapidly in time as the current increases.

the top and bottom electrode surfaces. However, ablation is free to occur in the rest of the simulation, and substantial currents flow in the vacuum region, wandering away from the rod. At this advanced stage, just at peak compression, the rod shows three distinct necks, spread over 5 mm along the rod axis. Plasma fingers have developed away from the rod surface, protruding inside the vacuum region.

We now cover the rod with a thin coating, 70 μm thick. This coating is 4 times less dense than aluminum, and the code computes the electrical resistivity of the coating from the Lee-More-Desjarlais model of aluminum, but with a mass density four times lower than solid aluminum. The simulation results are presented in Fig. 4(b), taken at the same time as Fig. 4(a). Now, the current is localized inside the rod. However, ablation is still present, and plasma fingers are developing next to the rod surface. The rod is not fully compressed at this time since the system is heavier. The ratio of the coating by rod volumes is 2 d/r, where d is the coating thickness and r is the rod

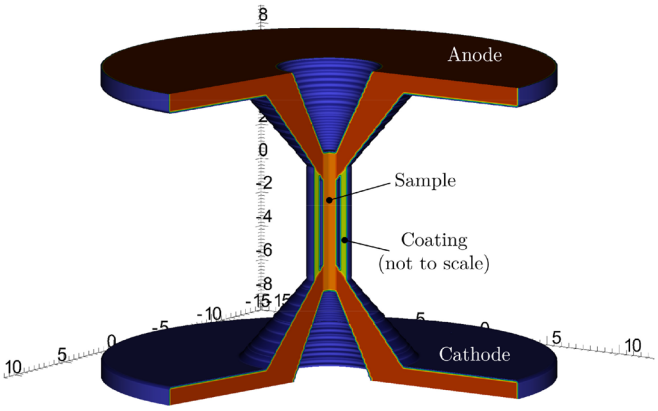

FIG. 3. A schematic view of the magnetic anvil cell. All sizes are in millimeters. The coating is not drawn to scale.

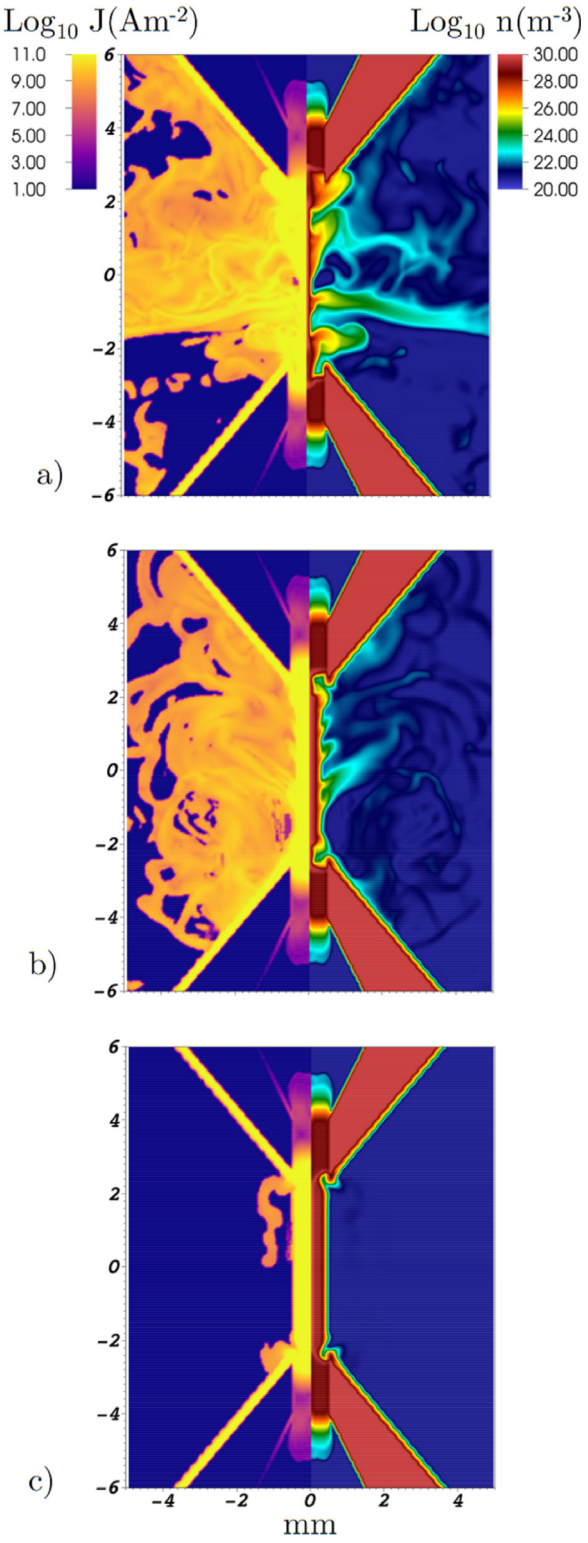

FIG. 4. Current density (left) and number density (right) for (a) no coating, (b) 70 μm coating, and (c) 140 μm coating 147 ns after the current starts.

radius. This corresponds to approximately 30% for this system, yielding a mass increase of 8% compared to the first case. When the coating is 140 μm thick, in Fig. 4(c), the ablation is completely quenched, and no current flows outside the rod. The magnetic field topology is now controlled by the initial geometry of the system. The ablation has been eliminated, and we can expect compression that is more homogeneous than with thinner coatings or when the coating is missing. However, the rod mass has increased by 16%, and the rod at this time is far from fully compressed. As expected from the previous case, the increase in mass has slowed down the pinch, and the coating becomes a limiting factor in the final properties that we can expect for warm dense matter.

Figure 5 now looks at maximum compression, when both rods are coated. When the coating is 70 μm thick, the rod, shown in Fig. 5(a), is fully compressed in 160 ns. There is very little plasma surrounding the rod. However, the low-density plasma is sufficient to allow the current to flow throughout the volume surrounding the rod. The highest current densities flow well outside of the compressed rod, reminiscent of the current distribution of Fig. 4(a). The edge of the rod near solid density [shown in dark orange on the right of Fig. 5(b)] is clearly not straight, hitting to inherent inhomogeneities inside the warm dense matter sample. While the coating was effective at limiting the ablation initially, it is clearly not thick enough to be considered very effective. When the coating thickness is doubled, Fig. 4(c) shows greater improvements. Looking now when the rod is fully compressed, we seem to have also a large volume filled with a low-density plasma. However, two subtle differences should be noted. First, the current flows mostly inside the rod. This is best seen by looking at regions where the current density is 10^{11} A/m^2 (i.e., brightest yellow) on the left of Fig. 5(c). Most of the current is still confined near the axis. We shall also emphasize that there are two clear gaps free of currents between both electrodes. All the current must flow through the rod to travel from the anode to the cathode. This is clearly not true in the other two cases. Second, the above-solid density region is virtually straight along the axis.

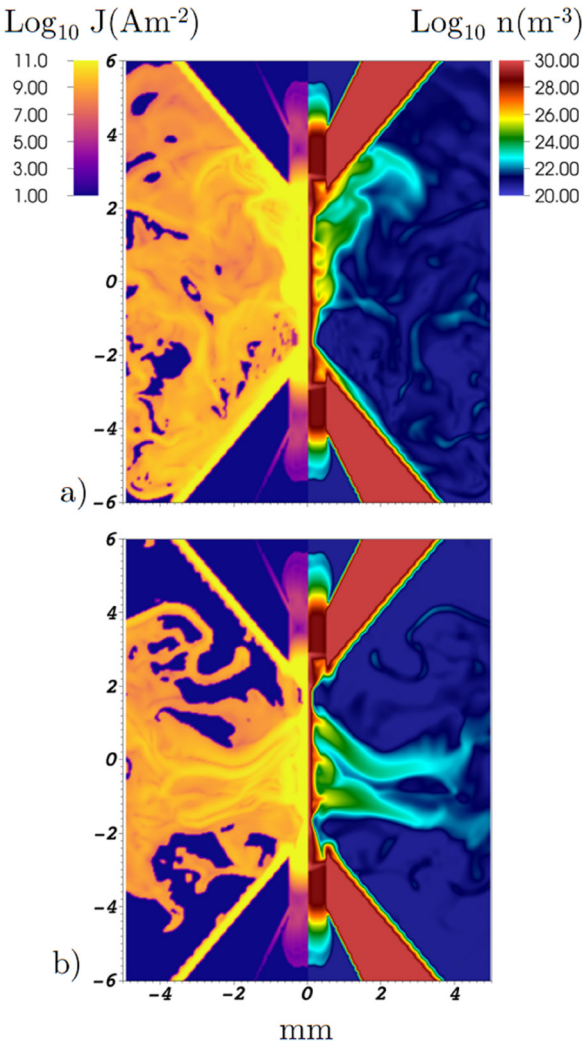

FIG. 5. Current density (left) and number density (right) for (a) 70 μm coating at 160 ns after the current starts and (b) 140 μm coating 180 ns after the current starts.

While these differences may impact the quality of the compression, they seem to be minor enough to barely matter. Yet, ablation occurring late triggers instabilities only when the current is decaying, and the strength of the magnetic field reduced. With thick coatings, most of the compression occurs in an environment devoid of spurious current paths. When currents start to deviate from the prescribed geometry, it is well after the current peak. As a result, coating only postpones instabilities, rather than eliminating them.

It is possible to measure quantitatively the impact of the coating on the quality of the warm dense matter sample by looking at the distribution of temperature vs. density for a volume limited to 1 mm above and below the midplane. The dynamics is clearly more disruptive near the electrodes. However, the properties do not have to be measured there. When using a pure z-pinch setup, devoid of coating, Fig. 6 shows a narrow dispersion in density, but a rather wide dispersion in temperature. It is very common for z-pinch pulsed-power

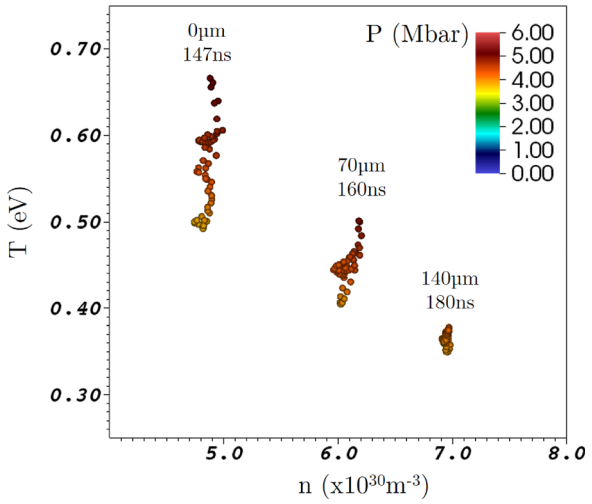

FIG. 6. Distribution of the temperature vs. the number density of the sample at maximum compression for three different coating thicknesses at maximum compression.

systems to develop electrothermal instabilities where the current flows in hotter, less resistive regions, giving rise to temperature conditions far from homogeneous. While small scale instabilities are not resolved in our simulation, the physical mechanisms responsible for current channeling are present in the MHD equations, and the direct effect is a relatively wide temperature distribution. When the rod is initially coated, the spread in temperature diminishes. A 70 μm thick coating reduces the distribution to +/–0.05 eV. A thicker layer brings the distribution to a mere 0.025 eV. The temperature drops with the increasing coating thickness. Starting at 0.6 eV, the temperature falls to 0.45 eV for the thinner coating down to 0.37 eV for the thicker coating. We have decided to keep the rod diameter the same in all three cases. As the coating thickness increases, the sample becomes heavier and the implosion is slower. We can recover high temperature by reducing the aluminum rod diameter slightly as we increase the coating thickness.

Given that the Coulomb coupling parameter

$$\Gamma_e = \frac{e}{4\pi\epsilon_0 T}\left(\frac{4\pi n_e}{3}\right)^{1/3} \tag{13}$$

is directly proportional to 1/T, where T is the temperature in V, but only proportional to $n_e^{1/3}$, large variation in temperature is more problematic than large variation in number density. This is also true for the Fermi degeneracy parameter

$$\Phi = \frac{\hbar^2\pi^2}{2eTm_e}\left(\frac{3n_e}{\pi}\right)^{2/3}. \tag{14}$$

A bare sample implosion gives a coupling that varies between 85 and 116 across the whole sample, while the degeneracy varies between 150 and 330. The thickest coating greatly reduces variations in Coulomb coupling, swinging between 168 and 183, and degeneracy, at 770 +/–30. We have assumed a constant ionization factor $Z_{eff} = 3$ in our computations. Clearly, the control of ablation also tightens the variations for these dimensionless parameters. It is important to note that simulations used the perfect gas approximation as the equation of state to minimize nonlinearities throughout compression. While the final pressure might be overestimated, this method gives ground to good comparison between all three cases presented in Fig. 6.

IV. CONCLUSIONS

The compression of the material sample required to obtain homogeneous and macroscopic samples of warm dense matter requires controlled conditions that preclude the growth of instabilities capable of mixing different states of matter together. While experimental evidence suggests that purely 3-dimensional instabilities can be mitigated since the convergence ratio is low, it was shown that 2-dimensional instabilities are still problematic for magnetic anvil cells when plasma ablation is present. Recent work showed that a thin coating effectively reduced the ablation of material surfaces of magnetic anvil cells, opening the way to study warm dense matter using pulsed-power generators. Without ablation, the current is forced to flow along the material surface, constraining magnetic fields to adopt a well-prescribed topology.

In this paper, we introduced a mass density scale length that highlights the impact of the plasma beta, resistivity, and mass density on the ablation rate. Two-fluid simulations using PERSEUS demonstrate that ablation is visibly reduced when the mass density of the coating is 4 times less than the mass density of the bulk material. The quality of the compression improves with the thickness of the coating. Thicker coatings tend to produce properties which are more homogeneous than thinner coatings. However, thicker coatings also limit the final temperature. Numerical simulations indicate that varying the mass density and the thickness of the coating can be an effective method to control the temperature of the sample at full compression.

In conclusion, we demonstrated numerically that a thin coating on material surfaces can greatly improve the quality of warm dense matter samples generated using pulsed-power generators. While one-fluid simulations usually give results that are more optimistic than experiments, two-fluid simulations show better predictive capabilities, especially in capturing plasma ablation.[36] While microscopic effects are perturbative and cause simulations to behave differently compared to experiments, it is important to remember that pulsed-power generators produce very large quantities of warm dense matter where microscopic effects should average out to what can be described as material properties at the mesoscale, the main reason for using pulsed-power generators in the first place.

ACKNOWLEDGMENTS

This research was supported in part by the NSF/DOE Partnership in Basic Plasma Science and Engineering via a DOE Office of Science, Fusion Energy Sciences Award DE-SC0016252, a DOE Office of Science, NNSA Award DE-NA0001944, and the NSF MRI Award PHY-1725178.

REFERENCES

[1]T. Guillot, D. J. Stevenson, W. B. Hubbard, and D. Saumon, in *Jupiter – the Planet, Satellites and Magnetosphere* edited by F. Bagenal, T. Dowling, and W. McKinnon (Cambridge University Press, New York, 2004), Chap. 3.
[2]R. Redmer, T. R. Mattsson, N. Nettelmann, and M. French, Icarus **211**, 798 (2011).
[3]J. J. Fortney, S. H. Glenzer, M. Koenig, B. Militzer, D. Saumon, and D. Valencia, Phys. Plasmas **16**, 041003 (2009).
[4]R. Nagler, B. Arnold, G. Bouchard, R. F. Boyce, R. M. Boyce, A. Callen, M. Campell, R. Curiel, E. Galtier, J. Garofoli, E. Granados, J. Hastings, G. Hays, P. Heimann, R. W. Lee, D. Milathianaki, L. Plummer, A. Schropp, A. Wallace, M. Welch, W. White, Z. Xing, J. Yin, J. Young, U. Zastrau, and H. J. Lee, "The matter in extreme conditions instrument at the Linac coherent light source," J. Synchrotron. Radiat. **22**, 520 (2015).
[5]B. G. Logan, F. M. Bieniosek, C. M. Celata, J. Coleman, W. Greenway, E. Henestroza, J. W. Kwan, E. P. Lee, M. Leitner, P. K. Roy, P. A. Seidl, J.-L. Vay, W. L. Waldron, S. S. Yu, J. J. Barnard, R. H. Cohen, A. Friedman, D. P. Grote, M. Kireeff Covo, A. W. Molvik, S. M. Lund, W. R. Meier, W. Sharp, R. C. Davidson, P. C. Efthimion, E. P. Gilson, L. Grisham, I. D. Kaganovich, H. Qin, A. B. Sefkow, E. A. Startsev, D. Welch, and C. Olsone, "Recent US advances in ion-beam-driven high energy density physics and heavy ion fusion," Nucl. Instrum. Methods Phys. Res. **577**, 1 (2007).
[6]L. B. Fletcher, H. J. Lee, T. Döppner, E. Galtier, B. Nagler, P. Heimann, C. Fortmann, S. LePape, T. Ma, M. Millot, A. Pak, D. Turnbull, D. A. Chapman, D. O. Gericke, J. Vorberger, T. White, G. Gregori, M. Wei, B. Barbrel, R. W. Falcone, C.-C. Kao, H. Nuhn, J. Welch, U. Zastrau, P. Neumayer, J. B. Hastings, and S. H. Glenzer, "Ultrabright X-ray laser scattering for dynamic warm dense matter physics," Nat. Photonics **9**, 274 (2015).
[7]A. N. Souza, D. J. Perkins, C. E. Starrett, D. Saumon, and S. B. Hansen, "Predictions of x-ray scattering spectra for warm dense matter," Phys. Rev. E **89**, 023108 (2014).
[8]D. Milathianaki, S. Boutet, G. J. Williams, A. Higginbotham, D. Ratner, A. E. Gleason, M. Messerschmidt, M. M. Seibert, D. C. Swift, P. Hering, J. Robinson,

W. E. White, and J. S. Wark, "Femtosecond visualization of lattice dynamics in shock-compressed matter," Science **342**, 220 (2013).
[9]B. Yu. Sharkov, D. H. H. Hoffmann, A. A. Golubev, and Y. Zhao, "High energy density physics with intense ion beams," Matter Radiat. Extremes **1**, 28 (2016).
[10]H. Reinholz, G. Röpke, S. Rosmej, and R. Redmer, "Conductivity of warm dense matter including electron-electron collisions," Phys. Rev. E **91**, 043105 (2015).
[11]B. Mahieu, N. Jourdain, K. Ta Phuoc, F. Dorchies, J.-P. Goddet, A. Lifschitz, P. Renaudin, and L. Lecherbourg, Nat. Commun. **9**, 3276 (2018).
[12]C. A. Ullrich, *Time-Dependent Density-Functional Theory: Concepts and Applications* (Oxford University Press, Oxford/New York, 2012).
[13]M. P. Desjarlais, J. D. Kress, and L. A. Collins, Phys. Rev. E **66**, 025401(R) (2002).
[14]S. Mazevet, M. P. Desjarlais, L. A. Collins, J. D. Kress, and N. H. Magee, Phys. Rev. E **71**, 016409 (2005).
[15]M. D. Knudson, D. L. Hanson, J. E. Bailey, C. A. Hall, J. R. Asay, and C. Deeney, "Principal Hugoniot, reverberating wave, and mechanical reshock measurements of liquid deuterium to 400 GPa using plate impact techniques," Phys. Rev. B **69**, 144209 (2004).
[16]R. W. Lemke, D. H. Dolan, D. G. Dalton, J. L. Brown, K. Tomlinson, G. R. Robertson, M. D. Knudson, E. Harding, A. E. Mattsson, J. H. Carpenter, R. R. Drake, K. Cochrane, B. E. Blue, A. C. Robinson, and T. R. Mattsson, "Probing off-Hugoniot states in Ta, Cu, and Al to 1000 GPa compression with magnetically driven liner implosions," J. Appl. Phys. **119**, 015904 (2016).
[17]T. Ao, R. Hickman, C. Hall, J. Asay, and S. Chantrenne, "The Veloce pulsed power generator for isentropic compression experiments," in *IEEE 34th International Conference on Plasma Science (ICOPS)*, Albuquerque, NM (2007), p. 203.
[18]T. Ao, J. R. Asay, S. Chantrenne, M. R. Baer, and C. A. Hall, "A compact stripline pulsed power generator for isentropic compression experiments," Rev. Sci. Instrum. **79**, 013903 (2008).
[19]B. Li, K. Bian, J. Matthew, D. Lane, K. M. Salerno, G. S. Grest, T. Ao, R. Hickman, J. Wise, Z. Wang, and H. Fan, "Superfast assembly and synthesis of gold nanostructures using nanosecond low-temperature compression via magnetic pulsed power," Nat. Commun. **8**, 14778 (2017).
[20]P.-A. Gourdain, A. B. Sefkow, and C. E. Seyler, "The generation of warm dense matter using a magnetic anvil cell," IEEE Trans. Plasma Sci. **46**, 3968 (2018).
[21]P.-A. Gourdain and C. E. Seyler, "The impact of three dimensional MHD instabilities on the generation of warm dense matter using a MA-class linear transformer driver," High Energy Density Phys. **24**, 50 (2017).
[22]K. J. Peterson, T. J. Awe, E. P. Yu, D. B. Sinars, E. S. Field, M. E. Cuneo, M. C. Herrmann, M. Savage, D. Schroen, K. Tomlinson, and C. Nakhleh, Phys. Rev. Lett. **112**, 135002 (2014).
[23]T. J. Awe, K. J. Peterson, E. P. Yu, R. D. McBride, D. B. Sinars, M. R. Gomez, C. A. Jennings, M. R. Martin, S. E. Rosenthal, D. G. Schroen, A. B. Sefkow, S. A. Slutz, K. Tomlinson, and R. A. Vesey, "Experimental demonstration of the stabilizing effect of dielectric coatings on magnetically accelerated imploding metallic liners," Phys. Rev. Lett. **116**, 065001 (2016).
[24]P.-A. Gourdain, "The generation of warm dense matter samples using fast magnetic compression," IEEE Trans. Plasma Sci. **43**, 2547 (2015).
[25]P.-A. Gourdain, A. B. Sefkow, and C. E. Seyler, "The generation of warm dense matter using magnetic anvil cells," Trans. Plasma Sci. **46**, 3968 (2018).
[26]M. Evans, M. B. Adams, P. C. Campbell, N. M. Jordan, S. M. Miller, N. B. Ramey, R. V. Shapovalov, J. Young, I. West-Abdallah, J. M. Woolstrum, R. D. McBride, and P.-A. Gourdain, "Reduction of ablated surface expansion in pulsed-power-driven experiments using an aerosol dielectric coating" Phys. Plasmas (submitted).
[27]H. Knoepfel, *Pulsed High Magnetic Fields* (North Holland Publishing Company, 1970), p. 93.
[28]P.-A. Gourdain, M. B. Adams, J. R. Davies, and C. E. Seyler, "Axial magnetic field injection in magnetized liner inertial fusion," Phys. Plasmas **24**, 102712 (2017).
[29]M. G. Haines, Proc. Phys. Soc. **74**, 576 (1959).
[30]M. G. Mazarakis, W. E. Fowler, A. A. Kim, V. A. Sinebryukhov, S. T. Rogowski, R. A. Sharpe, D. H. McDaniel, C. L. Olson, J. L. Porter, K. W. Struve, W. A. Stygar, and J. R. Woodworth, Phys. Rev. Spec. Top. Accel. Beams **12**, 050401 (2009).
[31]C. E. Seyler and M. R. Martin, "Relaxation model for extended magnetohydrodynamics: Comparison to magnetohydrodynamics for dense Z-pinches," Phys. Plasmas **18**, 012703 (2011).
[32]Y. T. Lee and R. M. More, Phys. Fluids **27**, 1273 (1984).
[33]M. P. Desjarlais, Controlled Plasma Phys. **41**, 267 (2001).
[34]P.-A. Gourdain, M. Evans, B. Foy, D. Mager, R. McBride, and R. Spielman, "HADES: A high amperage driver for extreme states," pre-print arXiv:1705.04411 (2017).
[35]M. R. Martin, C. E. Seyler, and J. B. Greenly, "The role of magnetic field in the transition to streaming ablation in wire arrays," Phys. Plasmas **17**, 052706 (2010).
[36]P.-A. Gourdain and C. E. Seyler, "Impact of the Hall effect on high-energy-density plasma jets," Phys. Rev. Lett. **110**, 015002 (2013).